Journal of Crystal Growth 76 (1986) 352–372
North-Holland, Amsterdam

GAS PHASE DEPLETION AND FLOW DYNAMICS IN HORIZONTAL MOCVD REACTORS

J. VAN DE VEN, G.M.J. RUTTEN *, M.J. RAAIJMAKERS and L.J. GILING

Department of Solid State Physics 3, Catholic University, Toernooiveld, 6525 ED Nijmegen, The Netherlands

Received 2 February 1986; manuscript received in final form 7 April 1986

Growth rates of GaAs in the MOCVD process have been studied as a function of both lateral and axial position in horizontal reactor cells with rectangular cross-sections. A model to describe growth rates in laminar flow systems on the basis of concentration profiles under diffusion controlled conditions has been developed. The derivation of the growth rate equations includes the definition of an entrance length for the concentration profile to develop. In this region, growth rates appear to decrease with the 1/3 power of the axial position. Beyond this region, an exponential decrease is found. For low Rayleigh number conditions, the present experimental results show a very satisfactory agreement with the model without parameter fitting for both rectangular and tapered cells, and with both H_2 and N_2 as carrier gases. Theory also predicts that uniform deposition can be obtained over large areas in the flow direction for tapered cells, which has indeed been achieved experimentally. The influence of top-cooling in the present MOCVD system has been considered in more detail. From the experimental results, conclusions could be drawn concerning the flow characteristics. For low Rayleigh numbers (present study $\lesssim 700$) it follows that growth rate distributions correspond with forced laminar flow characteristics. For relatively high Rayleigh numbers (present work > 1700–2800), free convective effects with vortex formation are important. These conclusions are not specific for the present system, but apply to horizontal cold-wall reactors in general. On the basis of the present observations, recommendations for a cell design to obtain large area homogeneous deposition have been formulated. In addition, this work supports the conclusion that the final decomposition of trimethylgallium in the MOCVD process mainly takes place at the hot substrate and susceptor and not in the gas phase.

1. Introduction

One of the most promising techniques for industrial processing of III–V compounds is metal-organic chemical vapor deposition (MOCVD). For this reason, much attention is paid to both fundamental and technical aspects of this growth technique at present. However, studies dealing with flow dynamics, depletion effects and cell design in MOCVD systems are very scarce.

Presently, many cell designs are based on the horizontal reactor. For this system, a number of both theoretical and experimental studies have been performed concerning the flow and temperature profiles and their development in the so-called entrance regions (e.g. refs. [1–8]). The Navier–Stokes partial differential equations which govern the transport phenomena in these systems can only be solved by numerical calculations for well defined conditions. Recently, such calculations were performed for laminar flow conditions [9–11]. Such treatments, however, are very elaborate and do not provide rapid insight into the physical processes when interpreting experimental observations. Therefore, simplified models to describe mass-transport and deposition rates in CVD are especially welcomed and used, frequently. These models often start from an analogy between temperature and velocity profiles and the concentration profile, of which the latter is established as the result of mass transport by diffusion and flow and chemical reactions. In such models, diffusion over a velocity boundary layer plays an important role, but in most cases the concentration profile has been simplified to a large degree. A review of various models is given in ref. [12]. On the basis of flow visualization experiments with TiO_2 particles, Eversteyn et al. [13] proposed a model in which a stagnant layer with constant thickness was assumed to be present above the susceptor. Over

* Present address: Semiconductor Development Laboratory, N.V. Philips, Nijmegen, The Netherlands

0022-0248/86/$03.50

this layer all temperature and concentration gradients in the cell were fully accomodated. Giling [6] showed that such stagnant layer theories are fundamentally not correct for laminar flow systems with low Rayleigh (Ra) and Reynolds (Re) numbers. For low values of the Ra number, a linear temperature profile is established between top and bottom of the cell. Kamotami and Ostrach [2] also showed that a stagnant layer, in which the linear gas velocity would be zero, is not present in a developed forced laminar flow profile. For high Ra numbers, often obtained when using N_2 or Ar as a carrier gas, the presence of a so-called "split-off" layer was shown [6]: a laminar boundary layer was found close to the susceptor with a strongly convective part above. It should be noted that such split-off layers can be the result of large entrance profiles, extending over a large part of the susceptor. In this entrance region large flow instabilities, such as return flows and vortex formation, may severely influence mass transport and, consequently, the positional distribution of growth rates. For these high Ra number systems a model involving an effective and constant diffusion boundary layer might be expected to explain the experimental observations.

In this study, only cells with rectangular ducts were used. In these reactors, under low Ra number conditions isotherms are parallel to the upper and lower cell boundaries when a top cooler is used [6]. Therefore, these cells are strongly preferred to cylindrical designs in which temperature gradients generally exist in lateral directions over the susceptor which may induce lateral gas motions and therewith influence growth rates. Recently, Houtman et al. [11] have shown by numerical computations that some vorticity may still be present in rectangular cells under low Ra number conditions due to the effect of the side walls. They also showed, however, that this did not affect temperature distributions in the cell, in accordance with experimental observations [6]. In the present work it will be shown that these vortex rolls have no effect on the mass transport phenomena, i.e. growth rates, either.

The present work mainly deals with mass transport phenomena in horizontal MOCVD reactors. Growth rates in these systems are controlled by gas phase transport of the III component via diffusion and flow [14]. A two-dimensional model describing the growth rate as a function of axial position is presented for laminar flow systems, based upon a consideration of concentration profiles in the cell. Growth rate results obtained in MOCVD of GaAs are confronted with this model for different experimental conditions. These include the use of H_2 and N_2 as carrier gases, various cell dimensions, water and air top cooling, various flow rates and gas phase concentrations of the growth components. Growth rates were also studied as a function of lateral position on the susceptor, to obtain information about possible lateral flow components [15]. Finally, some recommendations are given for the optimization of cell design to obtain homogeneous layer thicknesses on large surface areas and minimize gas phase depletion effects in MOCVD.

2. Model for diffusion controlled growth rates in a laminar flow system

In this section a model is presented to account for growth rates in horizontal CVD reactors, in which the deposition process is limited by mass-transport in the gas phase. The main idea of the model is that concentration profiles are calculated in the reactor, taking into account the flow profiles. The gas flow is considered to be laminar and dominated by forced convection. This implies that mixing effects due to free convective motions can be neglected. Return flow of heated gas may occur at the leading edge of the hot susceptor [16]. This is due to buoyancy forces caused by the expansion of the cold gases hitting the hot parts. This effect, which introduces additional mixing and memory effects, is neglected in the present model, too, but will be considered in more detail below qualitatively. The following treatment is two-dimensional. Symbols are defined in table 1.

2.1. Isothermal system

First, we consider a system with a constant temperature in which the active component rapidly decomposes at the susceptor, $y = 0$, for all axial

Table 1
List of important symbols

b	Total cell width
C	Concentration rate limiting component
C_0	Concentration rate limiting component at inlet
$\bar{C}(z)$	Average concentration rate limiting component at position z
d_h	Hydraulic diameter, $2bh/(b+h)$
D	Diffusion coefficient
D_0	Diffusion coefficient at 300 K
D_T	Diffusion coefficient at temperature T
G	Growth rate
Gr	Grashof number, Ra/Pr
h	Total cell height
M	Molecular weight growing crystal
N	Mass flux at susceptor
P_0	Input partial pressure rate limiting component
P_{AsH_3}	Input partial pressure of AsH_3
P_{TMG}	Input partial pressure of TMG
Pr	Prandtl number, $\nu/k \approx 0.7$ for gases, with ν kinematic viscosity, k thermal diffusivity
Ra	Rayleigh number, $g\beta\Delta T h^3/\nu k$, with g gravitational acceleration, β coefficient of volumetric expansion, $\Delta T = T_s - T_h$
Re	Reynolds number, $v_T d_h/\nu$
Sc	Schmidt number, ν/D
T_0	Reference temperature (this work: 300 K)
T_h	Temperature at upper wall ($y = h$)
T_m	Mean temperature
T_s	Temperature at susceptor ($y = 0$)
v	Gas velocity
v_0	Average gas velocity at reactor inlet at 300 K
v_T	Average gas velocity at temperature T
x	Lateral dimension
y	Height above susceptor
z	Axial dimension
z_0	Concentration entrance length
z_T	Temperature/flow entrance length, 0.4 Pr Re $h = 0.28$ Re h
θ	Tilting or tapering angle, also used as index
ρ	Density growing crystal

flow positions $z \geqslant 0$ (fig. 1a). Therefore, its concentration at $y = 0$ is zero for all values of z in the decomposition zone. Transport of material towards the susceptor in the y-direction goes entirely via diffusion (laminar flow). Transport in the flow direction is considered to be dominated by forced flow, i.e. diffusion in the axial direction is neglected in first instance. Later in the discussion of the experimental results, the effects of axial diffusion will be further considered. The

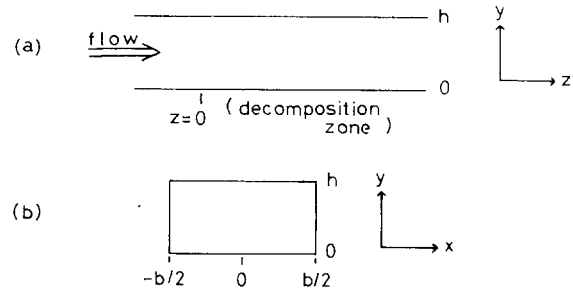

Fig. 1. Schematic cross sections of a reactor cell: (a) longitudinal: (b) transversal.

equation for mass conservation for this case is:

$$v(y)\frac{\partial C(y,z)}{\partial z} = D\frac{\partial^2 C(y,z)}{\partial y^2}, \tag{1}$$

in which D is the diffusion coefficient of the active component in the carrier gas and $v(y)$ expresses the parabolic velocity profile in the reactor as given by:

$$v(y) = 6v_0\left(\frac{y}{h} - \frac{y^2}{h^2}\right). \tag{2}$$

Eq. (1) is difficult to solve for a parabolic velocity profile. Therefore, we decided to take the following route: first solve the problem for a constant flow velocity and secondly consider the influence of a parabolic flow profile on the results obtained so far. For the case of a constant flow velocity (v_0) the problem can be solved analytically for the boundary conditions:

$$C(0, z) = 0, \quad \text{for all } z \geqslant 0, \tag{3a}$$

$$\left.\frac{\partial C(y,z)}{\partial y}\right|_{y=h} = 0, \quad \text{for all } z \geqslant 0, \tag{3b}$$

$$C(y, 0) = C_0, \quad \text{for all } 0 < y \leqslant h, \tag{3c}$$

The second condition (eq. (3b)) expresses that no mass-transport can occur through the upper wall of the reactor. Following the same lines as ref. [17], the above problem can be solved, giving:

$$C(y,z) = \frac{4C_0}{\pi}\sum_{m=0}^{\infty}\left\{\frac{1}{2m+1}\sin\left(\frac{2m+1}{2h}\pi y\right)\right.$$

$$\times \exp\left[\frac{-(2m+1)^2\pi^2 Dz}{4h^2 v_0}\right]\Bigg\}. \quad (4)$$

In this equation, m is a summation integer.

In fig. 2, concentration profiles at different positions z (in h^2v_0/D) are drawn as calculated from eq. (4). For small values of z the solution in eq. (4) is equivalent to an error function for diffusion in a semi-infinite medium. This holds until the concentration at $y = h$ falls significant below C_0. For the following analysis the critical concentration for this to happen is defined as $0.99C_0$. The axial distance z_0 at which the concentration at $y = h$ reaches this values can be calculated from eq. (4):

$$z_0 = h^2 v_0/16D. \quad (5)$$

It appears that for higher values of z, only the first term in the summation of eq. (4) has to be considered, as the series converges very rapidly. For these values of $z > z_0$:

$$C(y,z) = \frac{4C_0}{\pi} \sin\left(\frac{\pi y}{2h}\right) \exp\left(\frac{-\pi^2 Dz}{4h^2 v_0}\right). \quad (6)$$

In this equation, the gas phase depletion in the flow direction is represented by the exponential term. Eq. (6) also shows that the concentration profiles as a function of y have the same form for all values of $z > z_0$, as determined by the sine function. The distance z_0 can, therefore, be considered as an entrance length for the concentration profile to develop in the reactor cell: for $z \leqslant z_0$ the concentration profile has to build up and is the same as in a semi-infinite medium; for $z > z_0$ the concentration profile has developed and remains of the same form for all z.

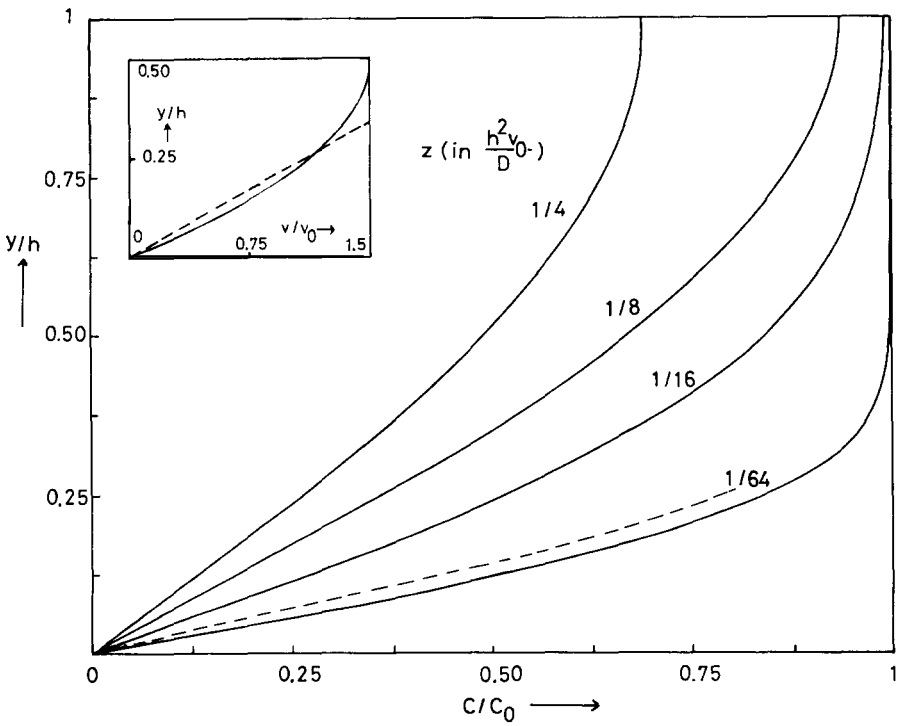

Fig. 2. (———) Concentration as a function of position above the susceptor in an isothermal cell with a capturing boundary at $y = 0$ and for a constant gas velocity. Parameter is the axial position, z (in h^2v_0/D). (– – –) Concentration profile for $z = h^2v_0/64D$ after correction for a linear velocity profile as described in the text. Insert: (———) Parabolic flow profile and (– – –) linear velocity approximation for $0 \leqslant y \leqslant h/4$.

2.2. Solutions for the development region $z \leqslant z_0$ in a linear flow profile

Fig. 2 shows that in the development region $z \leqslant z_0$ the largest drop in concentration occurs in a relatively thin layer above the susceptor. For calculation of the mass flux at $y = 0$, therefore, this part of the reactor represents the region of main interest. In fig. 2, it can be seen that the main concentration drop occurs between $y = 0$ and $y = h/4$. In order to solve eq. (1) in a more realistic way than the plug flow approach given above, the parabolic flow profile can be substituted by a linear velocity distribution:

$$v(y) = 4.5v_0(y/h), \tag{7}$$

which is on the average correct to within ~ 10% in the relevant range $0 \leqslant y \leqslant h/4$ (see insert fig. 2). Following ref. [18], the solution for a diffusion problem in a semi-infinite system with a capturing boundary at $y = 0$ and this linear velocity profile is given by:

$$\frac{C(y, z)}{C_0} = 1 - \frac{\int_\eta^\infty \exp(-a^3)\,\mathrm{d}a}{\Gamma(4/3)}, \tag{8}$$

where

$$\eta = y(v_0/2Dhz)^{1/3}.$$

Here, a is an integration parameter and Γ is the well known gamma function. The concentration profiles given by eq. (8) do not differ strongly from those given by eq. (4), but can be regarded as a refinement of the model. This is illustrated in fig. 2 for $z = h^2v_0/64D$ and $0 \leqslant y \leqslant h/4$.

Using Fick's law, the mass flux at $y = 0$, as given by

$$N(z) = -D\left[\partial C(y, z)/\partial y\right]_{y=0},$$

now becomes:

$$N(z) = 0.89DC_0(Dhz/v_0)^{-1/3}. \tag{9}$$

In terms of former models which equate for the mass flux $N(z) = DC_0/\delta$, the factor $(1/0.89)(Dhz/v_0)^{1/3}$ in eq. (9) can be considered as the effective boundary layer thickness. The error in the mass flux given in eq. (9) introduced by linear velocity profile is small (~ 3%), because of the 1/3 power in v_0. The mass flux follows a 1/3 power in z^{-1} and v_0 as a consequence of the linear velocity approximation.

Because the active component is only consumed at $y = 0$, the average concentration at $z = z_0$, $\bar{C}(z_0)$, can now be calculated on the basis of the total amount of material that has disappeared:

$$\int_0^{z_0} N(z)\,\mathrm{d}z = hv_0\left[C_0 - \bar{C}(z_0)\right]. \tag{10a}$$

Solution of this equation gives:

$$\bar{C}(z_0) = 0.79C_0. \tag{10b}$$

Using this and eqs. (9) and (5), we now obtain for the mass flux at $z = z_0$ ($y = 0$):

$$N(z_0) = 2.84D\,\bar{C}(z_0)/h. \tag{11a}$$

2.3. Solutions for the depletion region $z > z_0$.

Since the concentration profiles for values of z larger than the entrance length are of the same form (this will remain true for any velocity function which is constant in z), eq. (11a) can be generalized because of symmetry considerations:

$$N(z) = 2.84D\,\bar{C}(z)/h. \tag{11b}$$

The mass flux balance between the supply by forced flow and deposition at $y = 0$ for each z is now given by:

$$-hv_0\frac{\partial\bar{C}(z)}{\partial z} = 2.84D\frac{\bar{C}(z)}{h}. \tag{12}$$

Integration of this equation with respect to z from z_0 to z and with respect to $\bar{C}(z)$ from $0.79C_0$ to $\bar{C}(z)$ gives:

$$\bar{C}(z) = 0.79C_0\exp\left[\frac{-2.84D(z - z_0)}{h^2v_0}\right]. \tag{13}$$

The flux at $y = 0$ can now be calculated from eq. (11b). After rearranging, using eq. (5):

$$N(z) = \frac{2.68DC_0}{h}\exp\left(\frac{-2.84Dz}{h^2v_0}\right). \tag{14}$$

2.4. Growth rates in a cold-wall CVD reactor

Under experimental conditions, the lower cell wall ($y = 0$) is heated to a constant temperature, whereas the upper boundary ($y = h$) is water- or air-cooled. Since analytical calculations of the mass-fluxes in non-constant temperature fields are very difficult, an effective gas temperature is often introduced. It has been shown [19–22] that in systems similar to the present reactor cells, introduction of the arithmatic mean of the temperature gives a good approximation for the influence of temperature fields on the flux equations. Therefore, in a region of developed flow for the effective temperature the mean temperature in the cell can be taken:

$$T_m = \tfrac{1}{2}(T_s + T_h). \tag{15}$$

Here, T_s and T_h are the temperatures of the susceptor and the cooled upper wall, respectively. It can be argued that this mean temperature also is a good estimate for the entrance region, $z \leqslant z_0$.

The average velocity after thermal expansion, v_T, can be written in terms of T_m:

$$v_T = v_0\, T_m/T_0, \tag{16}$$

where T_0 and v_0 are the temperature and the average velocity of the gas in the cell before it hits the hot susceptor. Following refs. [21,22], the diffusion coefficient at elevated temperatures can be written as:

$$D_{T_m} = D_0(T_m/T_0)^{1.88}, \tag{17}$$

where D_0 is the diffusion coefficient at the reference temperature T_0. Substituting eqs. (15)–(17) into eqs. (5), (9) and (14), and using the ideal gas law for the (dilute) active component, the final equations for the flux $N(z)$ at $y = 0$ are obtained:

$0 \leqslant z \leqslant z_0$,

$$N(z) = \frac{0.89 D_0 P_0}{RT_m h}\left(\frac{T_m}{T_0}\right)^{1.88} \times \left[\frac{D_0}{v_0 h^2}\left(\frac{T_m}{T_0}\right)^{0.88} z\right]^{-1/3}, \tag{18a}$$

$z > z_0$,

$$N(z) = \frac{2.68 D_0 P_0}{RT_m h}\left(\frac{T_m}{T_0}\right)^{1.88} \times \exp\left[\frac{-2.84 D_0}{h^2 v_0}\left(\frac{T_m}{T_0}\right)^{0.88} z\right], \tag{18b}$$

with

$$z_0 = \frac{h^2 v_0}{16 D_0}\left(\frac{T_m}{T_0}\right)^{-0.88} \tag{18c}$$

Note that as reference temperature for the diffusion coefficient the cold gas temperature T_0 was taken. From the equations given above, the growth rate can easily be calculated using

$$G(z) = N(z) M/\rho, \tag{19}$$

where ρ is the density and M the molecular weight of the growing solid.

2.5. Tilted susceptor or tapered cell

For a tapered cell or a cell with a tilted susceptor, the free height above the susceptor is not constant. For a tilt angle of θ, it varies according to:

$$h_\theta(z) = h - z \tan\theta. \tag{20}$$

Here, h is the free height at the leading edge of the hot susceptor ($z = 0$). The average gas velocity increases with increasing z according to:

$$v_{0,\theta}(z) = v_0 h/(h - z \tan\theta). \tag{21}$$

In the entrance region, $z \leqslant z_0$, in general practice $z \tan\theta$ is small in comparison with h. The expressions for the mass flux in this region and the entrance length are then obtained in a good approximation by inserting eqs. (20) and (21) into eqs. (18a) and (18c):

$0 \leqslant z \leqslant z_{0,\theta}$,

$$N_\theta(z) = \frac{0.89 D_0 P_0}{RT_m}\left(\frac{T_m}{T_0}\right)^{1.88} \times \left[\frac{D_0(h - z\tan\theta)^2}{v_0 h}\left(\frac{T_m}{T_0}\right)^{0.88} z\right]^{-1/3}, \tag{22a}$$

$$z_{0,\theta} = \frac{z_0}{1 + (z_0 \tan\theta)/h}. \tag{22c}$$

Following the same lines as for a cell of constant height, integration of eq. (12) and insertion in eq. (11b) gives for the developed region:

$z > z_{0,\theta}$

$$N_\theta(z) = \frac{2.68 P_0 D_0}{R T_m (h - z \tan\theta)} \left(\frac{T_m}{T_0}\right)^{1.88} \times \exp\left[\frac{2.84 D_0}{v_0 h \tan\theta}\left(\frac{T_m}{T_0}\right)^{0.88} \times \ln\left(1 - \frac{z \tan\theta}{h}\right)\right]. \tag{22b}$$

From this equation it follows that a constant growth rate can be obtained in the developed region if the proper gas flow velocity is selected in combination with a certain value for θ, viz. if:

$$v_0 = \frac{2.84 D_0}{h \tan\theta}\left(\frac{T_m}{T_0}\right)^{0.88}. \tag{23a}$$

Then the growth rate is:

$z > z_{0,\theta}$,

$$G(z) = \frac{M}{\rho} \frac{2.68 P_0 D_0}{R T_m h}\left(\frac{T_m}{T_0}\right)^{1.88}. \tag{23b}$$

2.6. Entrance lengths

It is interesting to note that the entrance length for the concentration profile to develop, as given by eq. (18c), can be expressed in dimensionless Reynolds and Schmidt numbers using the definitions given in table 1:

$$z_0 = \tfrac{1}{16} \mathrm{Re}\ \mathrm{Sc}\ h \tag{24a}$$

To arrive at this expression, the hydraulic diameter appearing in the expression for Re is approximated by free height above the susceptor, h. Eq. (24a) has the same structure as the expression for the thermal entry length for laminar flow as given in refs. [1,2,6]:

$$z_T = 0.40\ \mathrm{Re}\ \mathrm{Pr}\ h. \tag{24b}$$

Here, Pr is the Prandtl number which for gases has a value of ~ 0.7 at all relevant temperatures. Since the Schmidt number generally is ~ 3 times larger than Pr for H_2 and N_2, in the heated region the thermal entry length (and coupled to that the velocity entry length) is 2–3 times larger than the concentration entrance length. This implies that whenever strong thermal entrance effects are present which can significantly disturb the concentration profile (e.g. cold finger, return flow), the practically observed concentration entrance length is expected to be larger than z_0 and to approach z_T (see sections 5.1.2 and 6.1).

3. Experimental

Experiments were performed in quartz cells with rectangular cross-sections. Unless otherwise stated, they were water-cooled at the top and air-cooled at the side walls (fig. 3). In some cases, a fully air-cooled design was used. The cell was resistance heated at the bottom. To maintain homogeneity of the temperature at the heated parts, a main/slave system with two independent elements was used. Additionally, an element was available to preheat the gases before these hit the hot susceptor. Preheater temperatures up to $\sim$ 350°C were found not to influence the results in the deposition zone. For higher temperatures decomposition of reactive gases occured in the preheater zone. Therefore, the preheater option was not used in the present MOCVD experiments. Temperatures were measured with a calibrated optical pyrometer at the crystal surfaces and were found to be constant to within ± 5°C. In the present experiments, a fixed susceptor temperature of 700°C was used. During MOCVD, an arsenic film was deposited at the top cell wall. Due to reflection of infrared radiation at this film, considerable temperature changes were observed at the susceptor in the course of an experiment. This effect was efficiently removed by depositing a metallic silver mirror at the bottom of the (top) water-cooler (fig. 3).

As susceptor a 0.2 cm thick quartz plate was used with the same width as the reactor cell to avoid dead volumes and possible formation of flow eddied between the susceptor edge and cell

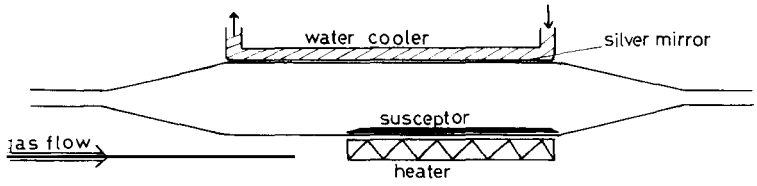

Fig. 3. Cell with top water-cooler.

wall. All gas line to cell transitions were realized with an angle smaller than 7° to avoid eddy formation [23]. The width ofthe cells was kept constant at 5.0 cm. The free height above the susceptor was varied from 0.8 to 3.8 cm. A cell with a tapering angle of 3.5° was used with a free height at the leading edge of the hot susceptor of 2.1 cm. The inlet region before the deposition zone (fig. 3) was ~ 14.0 cm in all cells. It was calculated that this allowed the velocity profile to establish in all cases [24]. The hot zone suited for epitaxial growth was ~ 20.0 cm in length. The transition from the (cold) inlet region to the growth region at 700°C was found to occur within approximately 2 cm. The position $z = 0$, defining the leading edge of the hot susceptor, was taken at the centre of this zone.

As carrier gases pure H_2 and N_2 were used, with a water and oxygen content below the ppm level. Flow rates varied between 0.75 and 9 SLM. As growth components arsine ("Phoenix-grade" from Matheson) and trimethylgallium (TMG) ("electronic grade" from Alfa Ventron) were used, with an input partial pressure ratio P_{AsH_3}/P_{TMG} = 15–20. The maximum TMG partial pressure used was 90 Pa. All experiments were performed at atmospheric pressure.

Single crystalline GaAs substrates with a thickness of 250–300 μm, {100} oriented with a misorientation of 0° or 2° towards {110} were used. Misorientation, dopant type and dopant level were found not to influence the growth rates measurably. Before loading into the reactor, samples were first chemo-mechanically polished. Successively they were degreased in ultrasonically stirred chloroform and acetone baths, dipped in a diluted HCl solution and extensively rinsed in pure, 0.2 μm dust filtered, water with a conductivity of ~ 0.1 μS. Finally, they were blown dry in a nitrogen stream. After growth, thicknesses of epitaxial layers were evaluated by cleaving the samples and etching off ~ 0.2 μm of the cross sections in a CrO_3–HF solution under illumination [25]. The latter treatment reveals the substrate/epitaxial layer interface excellently. The layer thickness can successively be evaluated under an optical microscope. Growth rates can be measured by this method with an inaccuracy of ±5–10%, depending on the layer thickness.

4. Application of the diffusion model to the MOCVD process

It is a generally accepted fact that the growth rate of GaAs during MOCVD in hydrogen is limited by gas phase diffusion of the Ga component (e.g., ref. [14]). The arguments leading to this conclusion include the independence of the growth rate on temperature and partial pressure of arsine (P_{AsH_3}) within wide limits and the linear dependence on the partial pressure of trimethylgallium (P_{TMG}). Since the same arguments are valid when nitrogen is used as a carrier gas (present work (not shown) and ref. [26]), the growth rate is concluded to be diffusion controlled also in this case. In the present work, the conclusions given above were found to hold for all axial positions in the deposition zone.

TMG is known to decompose rapidly in H_2 and N_2 at temperatures above ~ 420 and ~ 570°C, respectively [27]. Therefore, when top water-cooling is used decomposition is only expected in the lower part of the cell. In pure hydrogen, liquid gallium is formed under these conditions on both the quartz susceptor and GaAs substrates. In pure nitrogen, gallium droplets are formed on GaAs surfaces only, while on the susceptor a chemically very resistant (polymeric) film

is deposited. Evidently, under these conditions the crystal surface effectively catalyzes the gallium-methyl species arriving at the bottom of the cell to form elemental gallium. This shows, that in a N_2 atmosphere the TMG molecule cannot be fully decomposed in the gas phase, as was suggested previously [27]. A similar conclusion could also be drawn for H_2 as a carrier gas from a study of carbon incorporation in GaAs layers [28] and from a comparison of incorporation rates of the III elements in III–V epitaxial layers when using various metalorganic compounds [29]. In this work, further proof will be given to this conclusion. During MOCVD, both in H_2 and in N_2, growth rates were found not to be influenced noticeably by the substrate surface area upstream. This was checked in several experiments by measuring growth rates at different axial positions z with and without other substrates in the upstream part of the reactor. Therefore, we conclude that the TMG decomposition rate was equal at all positions on the (hot) susceptor, independent of the presence of GaAs substrate material.

From the above, we conclude that under forced laminar flow conditions, the theoretical model which was discussed above should be applicable to the present system. Although the nature of the diffusing species is not completely clear, in the present analyis the diffusion coefficients for the undecomposed TMG molecule are used. They were calculated using the expression for the binary diffusion coefficient [30] and physical constants for TMG, H_2 and N_2 [30,31]. In H_2 and N_2 the following values were obtained for 300 K (also using eq. (17)):

$$D_0^{H_2} = 0.378 \text{ cm}^2/\text{s}, \quad D_0^{N_2} = 0.091 \text{ cm}^2/\text{s}.$$

Since these diffusion coefficients vary approximately with the square root of the reduced molecular mass of the diffusing molecules, only small differences for the diffusion of the various possible gallium–methyl species are expected.

5. Results

In table 2, the main parameters describing the gas flow dynamics in the present experiments are given. In the fifth column the maximum and minimum flow velocities are given which were used in a specific cell, calculated for a reference temperature of 300 K. In case of water top cooling, the temperature at the upper wall is assumed to be ~ 400 K [7] and for the mean gas temperature a value of 700 K was adopted. For the air-cooled cell a temperature of ~ 700 K was measured at the upper wall and for the mean gas temperature a value of 850 K was adopted. These values are not critical for further theoretical calculation of growth rates (eqs. (18) and (22)) within wide (50 K) limits. All parameters in table 2 were calculated for these temperatures using data from ref. [32]. For cell D the upper-wall temperature is expected to be lower than in the other cells [7]. This influences the Ra number considerably, as it varies with $T^{4.4}$ [6]. Since for cell D with H_2 as a carrier gas Ra is close to the critical value of 1700, for this case Ra number values are given as calculated for upper-wall temperatures of 300 to 400 K. Note that Re and the entrance lengths are proportional to the input gas velocity, v_0.

From the table it is clear, that in all practical cases the Reynolds number is well below the limit of 2300, at which a transition from laminar to turbulent flow occurs [33]. The Rayleigh number, however, which has a critical value of 1700 at which a transition from forced flow to flow with free convective effects is expected to occur [6,34,35] changed considerably in our experiments. Giling [6] found by interference holography studies that the Ra number is the main parameter describing convective instabilities in the reactor. Therefore, in the present paper results will be presented for systems with low (< 1700) and high (> 1700) Ra numbers, separately. Unless otherwise stated, experimentally determined growth rates refer to the centre of the susceptor, i.e. $x = 0$ (fig. 1b). Variation of growth rates across the width of the susceptor are discussed in a separate section. This paper will not deal with morphology of the grown epitaxial layers. It should be remarked, however, that mirrorlike surfaces were obtained in almost all cases. As an exception, crystals which were grown in the first 2–3 cm from the leading edge of the susceptor often showed features typical of low temperature growth [36]. Other aspects of

Table 2
Main parameters describing the flow characteristics in the present experiments

Cell	h (cm)	d_h (cm)	b/h	v_0 cm/s	H_2 Re	H_2 Ra	H_2 $\frac{Gr}{Re^2}$	H_2 z_T (cm)	H_2 z_0 (cm)	N_2 Re	N_2 Ra	N_2 $\frac{Gr}{Re^2}$	N_2 z_T (cm)	N_2 z_0 (cm)
A	0.8	1.4	6.3	3.4	2.4	15	3.6	0.5	0.2	16	700	3.6	3.7	0.7
				10.3	7.4		0.4	1.6	0.5	50		0.4	11.5	2.2
B	1.8	2.6	2.8	2.1	2.7	170	32	1.3	0.5	19	8000	32	9.7	2.2
				12.2	16		0.9	7.7	3.1	110		0.9	56	13
C	2.9	3.7	1.7	1.9	–	–	–	–	–	24	33500	80	20	5.2
				5.7						75		8.2	60	16
D	3.9	4.4	1.3	2.8	6.4	1720–2800	58	6.5	3.3	–	–	–	–	–
				8.7	20		5.9	20	10.4					
B*	1.8	2.6	2.8	2.1	2.4	40	9.6	1.1	0.4	–	–	–	–	–
				9.2	10.6		0.5	5.0	2.0					

B* refers to air-cooled cell; other cells are top water-cooled. Cell width (b) is constant: 5.0 cm. For further explanation: see text and table 1.

MOCVD growth on large surface areas, such as uniformity of electrical and optical properties, will be dealt with in a future paper [28].

5.1. Experiments under low Ra number conditions

5.1.1. H_2, cell B

In figs. 4a–4c, growth rates are given as a function of input arsine pressure, susceptor temperature and input TMG pressure. The latter plot includes curves for three different axial positions. The dashed lines in these plots are growth rates calculated with eqs. (18) and (19) without a parameter fit. Since the arsine partial pressure does not appear in these expressions, growth rates are expected to be independent of this parameter. The data calculated on the basis of the (diffusion) model agree very well with the experimental results. It is clear that the experimental curves show a behaviour typical of the MOCVD process: growth rates are independent of arsine input pres-

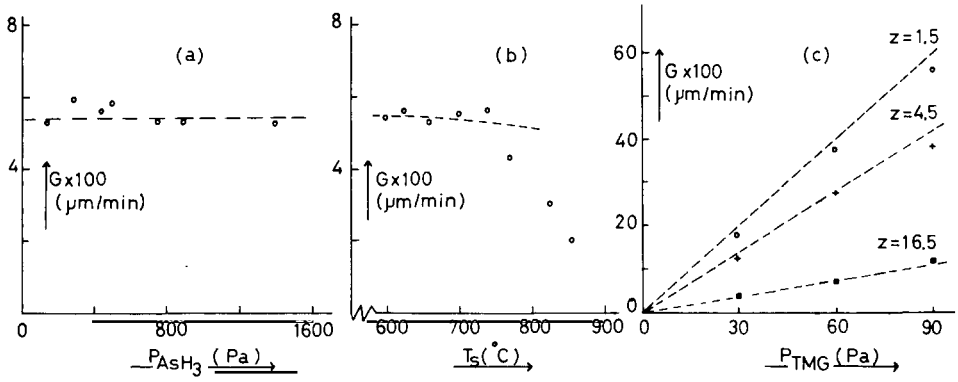

Fig. 4. GaAs growth rates (G) at $x = 0$ in cell B, with H_2 as a carrier gas and an input gas velocity $v_0 = 6.1$ cm/s, as a function of: (a) input arsine pressure, P_{AsH_3}, for $P_{TMG} = 30$ Pa and $z = 13$ cm: (b) susceptor temperature, T_s, for $P_{TMG} = 30$ Pa and $z = 13$ cm; (c) input TMG pressure, P_{TMG}, at $z = 1.5$ (○), $z = 4.5$ (+) and $z = 16.5$ cm (■). (– – –) Calculated curves.

sure and temperature within wide limits and vary linearly with P_{TMG}. The fall in growth rate above ~ 750°C most probably is due to desorption of the gallium growth component from the surface [37].

In fig. 5 both experimental and calculated growth rates are given as a function of axial position in the reactor, z, for three flow rates. In these plots the calculated entrance lengths for the concentration profile are indicated. The calculated data fit well with the experimental results for the lower flow rates. The agreement is less, but still very acceptable, for higher gas velocities. From the curves it is evident that G varies strongly along the length of the susceptor in all cases: gas phase depletion causes an exponentially decaying deposition rate.

5.1.2. N_2 and H_2, cell A

In this cell, for both hydrogen and nitrogen as carrier gases, the same dependence of growth rate on P_{AsH_3}, T_s and P_{TMG} was found as in cell B for H_2. In fig. 6 growth rates in N_2 are given as a function in z for three flow velocities. Though calculated deposition rates are somewhat lower than those experimentally observed, it can be concluded that the agreement between the model and the measured data is very acceptable for the lower flow rates used. It should be noted in this respect that in these experiments the estimated maximum inaccuracy in allocation of the $z = 0$ position where decomposition of TMG started was ~ 1 cm. By shifting experimental and calculated curves over this distance, a large improvement in overlap can be achieved. For higher flow velocities and low values of z, experimental growth rates are considerably higher than those calculated on the basis of eqs. (18) and (19) (fig. 6c).

In hydrogen, rapid gas phase depletion occurs in this cell A (fig. 7). This growth rate decay is much faster than in N_2, since the diffusion coefficient of the active component is much higher in

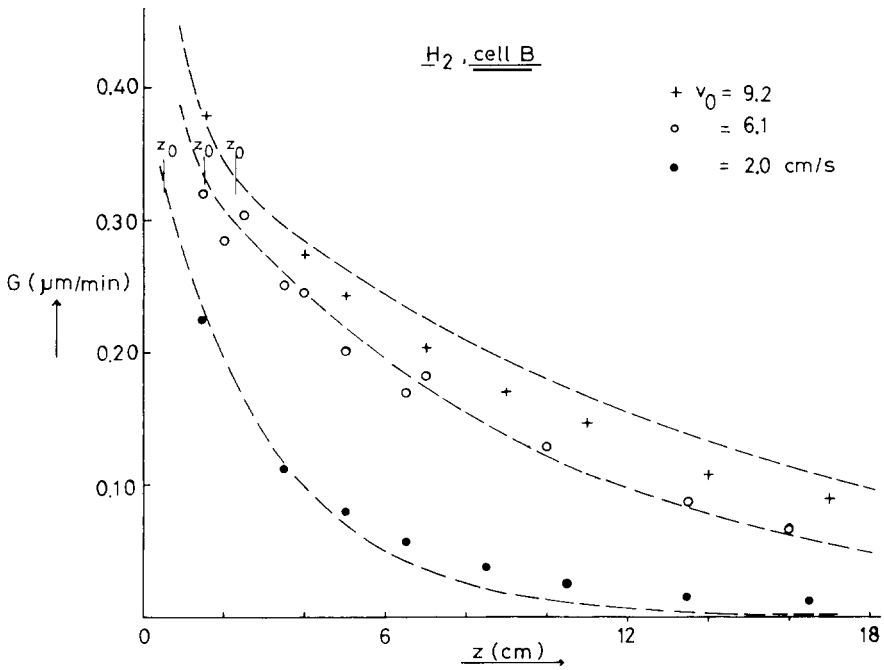

Fig. 5. GaAs growth rates (G) at $x = 0$ in cell B with H_2 as a carrier gas and $P_{TMG} = 50$ Pa as a function of axial position, z. (+), (○), (●) Experimental data points for input flow velocities of 9.2, 6.1 and 2.0 cm/s, respectively. (– –) Calculated curves; the concentration entrance lengths are indicated by z_0.

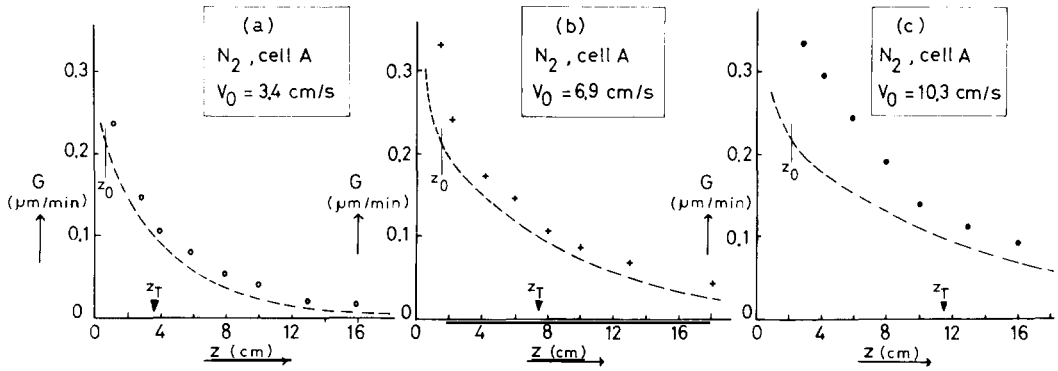

Fig. 6. GaAs growth rates (G) at $x = 0$ in cell A with N_2 as a carrier gas and $P_{TMG} = 60$ Pa as a function of axial position z for three input flow velocities: (a) 3.4 cm/s; (b) 6.9 cm/s; (c) 10.3 cm/s. (– – –) Calculated curves; concentration and temperature entrance lengths are indicated by z_0 and z_T, respectively.

H_2 than in N_2. Fig. 7 shows that the decay which is predicted from the model is stronger than experimentally observed. Logarithmic plots of measured growth rates versus z for $z > z_0$ showed straight lines for all flow velocities used. The slopes of these lines were 40% (±7%) of those calculated on the basis of eq. (18). This phenomenon can be attributed to diffusion in the axial flow direction due to the very large concentration gradients and will be discussed in more detail below.

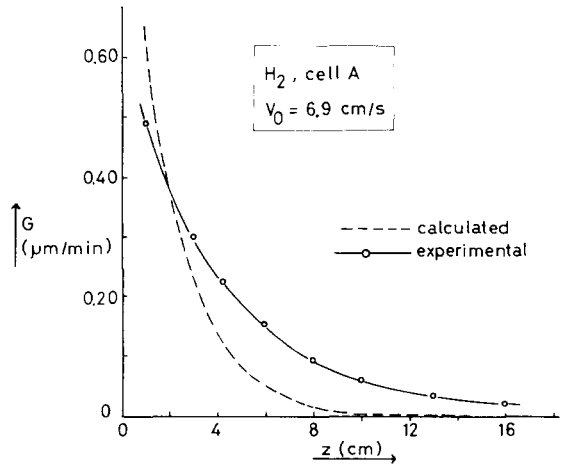

Fig. 7. GaAs growth rates (G) at $x = 0$ in cell A as a function of axial position z with H_2 as a carrier gas, input gas velocity 6.9 cm/s and $P_{TMG} = 60$ Pa. (– – –) Calculated curve.

5.1.3. Lateral homogeneity

Growth rates were also studied as a function of the lateral position x on the susceptor (fig. 1b) by placing rows of GaAs substrates perpendicular to the main gas flow. As a typical example, results obtained in cell B with H_2 as a carrier gas and in cell A with N_2 as a carrier gas are shown in fig. 8. These results show that, except for the first centimetres on the susceptor, growth rates are constant to within ±5% for at least 70% of the width of the cell. For higher gas flow velocities in cell B, this value was found to be slightly lower (~ 50%).

5.1.4. Air-cooled cell B

In case of air-cooling, growth rates were found to decay more rapidly than in top water-cooled cells. As a typical example, a plot of growth rates versus position z is given in fig. 9 for a H_2 gas flow velocity of 6.1 cm/s. The logarithmic plot in the insert shows that for $z > z_0$ the curve consists of two exponential parts. For z-values smaller than ~ 5 cm, the slope is 0.13. This value is in excellent agreement with the value of 0.135, which is calculated from eq. (18) using a mean gas temperature of 850 K as discussed before. For larger values of z, a slope of 0.28 is obtained from fig. 9. This means that the term in the exponent is doubled for these axial positions and that the gas phase depletion is two times faster. From this, we conclude that in this part of the cell TMG decom-

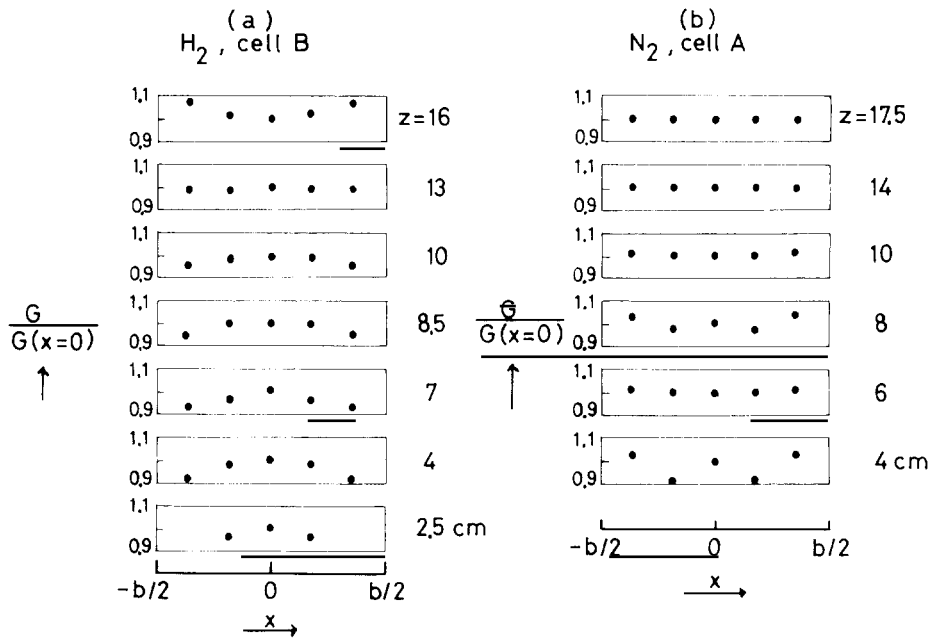

Fig. 8. Lateral growth rate distributions in cell B with H_2 as a carrier gas (a) and cell A with N_2 as a carrier gas (b) for various axial positions, z. Input gas velocities were 6.1 and 4.6 cm/s, respectively.

position occurred at both the susceptor and the upper wall of the reactor.

The critical position at which the doubling of the exponent occurred was of the same order as the entrance length for the temperature profile (compare, e.g., fig. 9 and table 2). TMG decomposition in H_2 starts to be important for temperatures higher than $\sim 400°C$ and is complete at $\sim 460°C$ [27]. In the present case, a temperature of 700 K was measured at the upper wall of the cell in the developed region. Therefore, for z-values smaller than the thermal entrance length, TMG decomposition is only expected at the bottom of the cell, since the temperature at $y = h$ still is too low [1,2]. For more downstream axial positions, however, this reaction also occurs at the upper wall and depletion of the gas phase is two times faster. The present experimental results confirm the earlier given conclusions on the decomposition of TMG, viz. that this reaction only occurs at the hot surface and not in the gas phase (see also, e.g., ref. [37]).

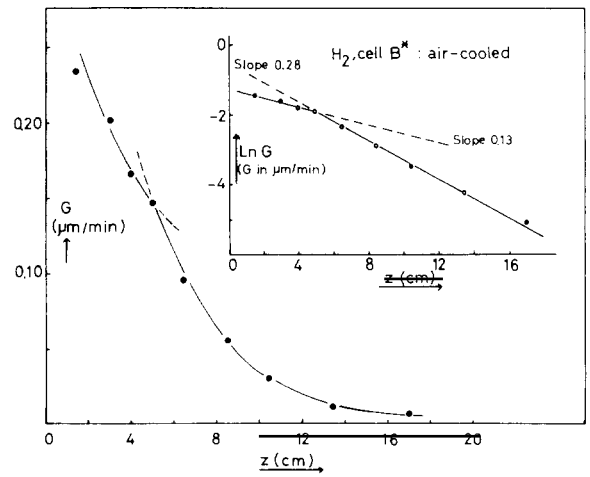

Fig. 9. GaAs growth rates (G) at $x = 0$ as a function of axial position (z) in cell B without top water-cooling (air-cooled), H_2 as a carrier gas, $v_0 = 6.1$ cm/s and $P_{TMG} = 30$ Pa. Insert: Logarithmic plot.

5.2. Experiments under high Ra number conditions

In cells where, because of the large height, free convection vortices are expected to develop, growth rates were found to show similar behaviour with varying P_{AsH_3}, T_s and P_{TMG} as for systems with low Ra numbers (fig. 4). The rates predicted by the diffusion model for laminar flow, however, deviate strongly from those which were experimentally observed. In fig. 10 measured growth rates in H_2 are plotted as a function of axial position, z, in cell D at $x = 0$ for gas velocities (v_0) of 2.9, 5.8 and 8.7 cm/s, respectively. For comparison, growth rates calculated with eq. (18) for $v_0 = 5.8$ cm/s are also included.

For higher flow rates, growth rates tend to become constant in the upstream part of the reactor (fig. 10). The same entrance effect was found when N_2 was used as a carrier gas, though the entrance lengths were larger. In all cases, the above mentioned effect occurred within in a distance from the leading edge of the susceptor which was of the order of the entrance lengths for the concentration and temperature profiles (z_0 and z_T, respectively).

Beyond the above mentioned entrance regions, growth rates were found to decay exponentially but not according to eq. (18). From logarithmic plots of the growth rates versus axial positions, effective diffusion boundary layer thicknesses, δ_{eff}, were calculated for this downstream region, assuming a constant value of δ as used in the stagnant layer model of Eversteyn and coworkers [13]. For all flow rates used, for both H_2 and N_2 as carrier gases, the value of δ_{eff} was found to vary between 0.15 and 0.25 cm. This δ-value, however, can only be used to describe growth rates at the centre line of the susceptor (i.e. $x = 0$), since G was found to vary strongly across the width of the cell. This effect is illustrated in figs. 11 and 12. Here, growth rates are shown as a function of axial position z for different lateral positions x, using a H_2 flow of 2.9 cm/s in cell D (fig. 11) and a N_2 flow of 6.1 cm/s in cell B (fig. 12). For H_2 in cell D, neglecting small values of z, growth rates in the central part of the cell are lower than at the edge of the susceptor. The reverse is true for N_2 in cell B. These results show the presence of vortex motions in the cell, which will be discussed in more detail below.

Under comparable experimental conditions, both from flow visualization experiments per-

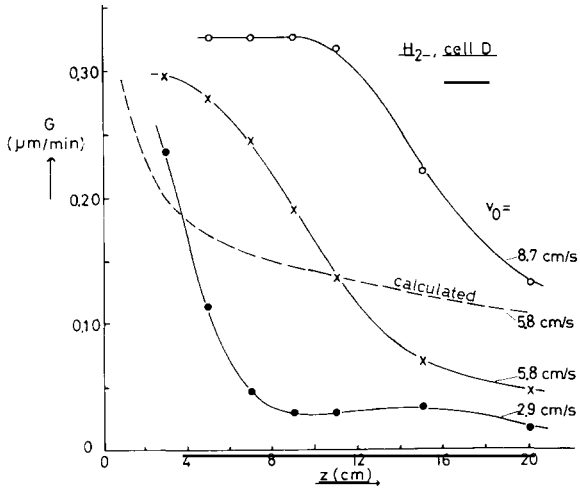

Fig. 10. GaAs growth rates (G) at $x = 0$ as a function of axial position (z) in cell D with H_2 as a carrier gas and $P_{TMG} = 50$ Pa. Input gas velocities are 2.9, 5.8 and 8.7 cm/s, respectively. (– – –) Calculated with eq. (18) for for 5.8 cm/s.

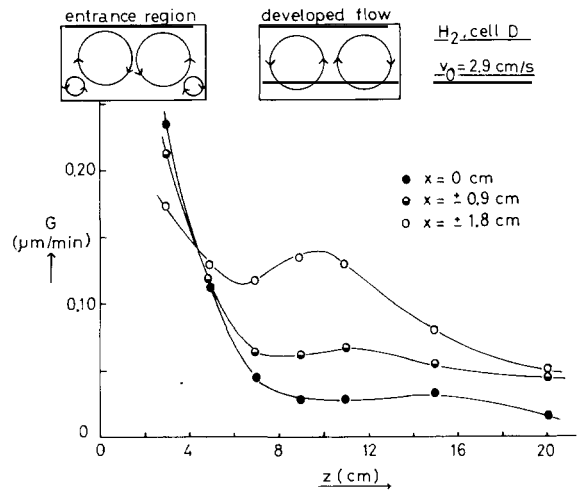

Fig. 11. GaAs growth rates (G) as a function of axial position (z) for different lateral positions (x) in cell D with H_2 as a carrier gas, input flow velocity 2.9 cm/s, $P_{TMG} = 50$ Pa. Inserts: Vortex motions.

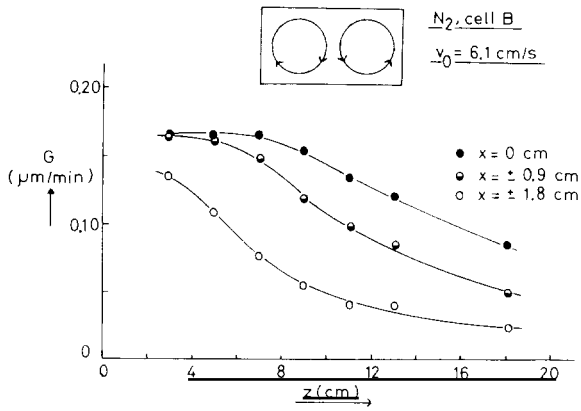

Fig. 12. GaAs growth rates (G) as a function of axial position (z) for different lateral positions (x) in cell B with N_2 as a carrier gas, input flow velocity 6.1 cm/s $P_{TMG} = 50$ Pa. Insert: Vortex motions.

formed by Eversteyn et al. [13] and holographic measurements by Giling [6], a much thicker split-off boundary layer was found ($\delta \approx 0.8$ cm or more). Both from this and from the strong lateral variation in growth rates we conclude that the presently observed effective boundary layer has no physical meaning, but merely is a parameter describing the decay of growth rates at $x = 0$.

5.3. Experiments in a tapered cell

Experiments were performed in a tapered cell with a tapering angle of 3.5°, using both hydrogen and nitrogen as carrier gases. The free height at the leading edge of the susceptor was 2.1 cm. Therefore, results can be compared with those obtained in cell B, which has a free height above the susceptor of 1.8 cm (table 2). The angle of 3.5° was selected as a compromise to achieve a reasonable input gas velocity at which the growth rates are expected to be constant (eq. (23)), and to obtain a large deposition zone.

Fig. 13 shows plots of the growth rate in H_2 as a function of axial position for three flow velocities. The dashed lines in these plots were calculated on the basis of eqs. (22) and (19). In the

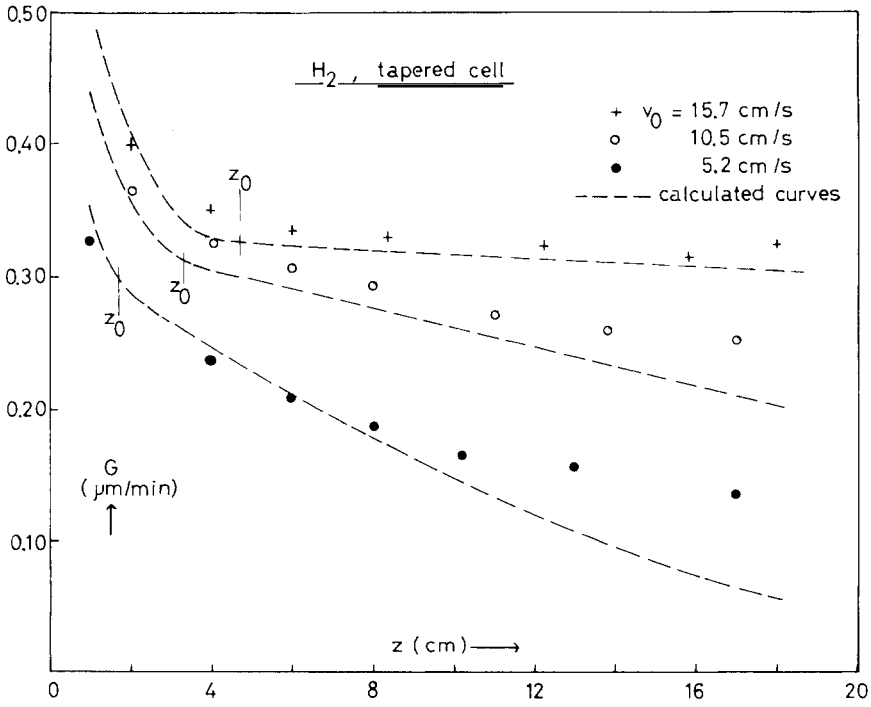

Fig. 13. GaAs growth rates (G) at $x = 0$ in a 3.5° tapered cell with H_2 as a carrier gas and $P_{TMG} = 50$ Pa as a function of axial position (z) for input gas velocities of 5.2, 10.5 and 15.7 cm/s. (– – –) Calculated on the basis of eqs. (22) and (19).

entrance region ($z \leqslant z_{0,\theta}$), growth rates decreased strongly with increasing z, also in this tapered cell. For larger values of z, growth rates became constant when the proper gas flow velocity was selected. The agreement between the experimental results and the calculated curves is very reasonable: both the form of the curves and the absolute values for the growth rate are predicted well by eqs. (22) and (19).

Under the present conditions, the lateral distribution of growth rates was essentially the same as in cell B, although the homogeneity generally was slightly less. For the highest H_2 flow rates used in the tapered cell, homogenous deposition to within $\pm 5\%$ was obtained over ~ 40–50% of the susceptor width. Recent experiments in slightly modified tapered cells, however, indicate that this homogeneity can still be improved. This subject will be treated in a future paper.

Using this tapered cell has only a minor effect with nitrogen as carrier gas: apart from relatively small differences in absolute values of growth rates, the axial growth rate distributions in the tapered cell were essentially the same as those obtained in a non-tapered cell. Additionally, the lateral distribution of growth rates was essentially the same in these two cases, viz. no homogeneous deposition across the width of the cell and higher growth rates in the centre of the susceptor as compared with the edges.

6. Discussion

6.1. Low Ra numbers: validity of the model for laminar flow

From the results it can be concluded that in most cases a very acceptable fit between experimental growth rates and values calculated with the model has been obtained for systems with low Ra numbers. It should be emphasized that despite the simplifying assumptions made in the model, these results were obtained without optimization of parameters.

Perhaps one of the most important simplifications in the derivation of the final growth rate equations was the neglect of the Soret effect. Following the same lines as Bloem [38] and using theoretical data from Grew and Ibbs [39], the thermal diffusion effect was calculated to give an effective lowering of the TMG diffusion coefficient of $\sim 20\%$ in the present cases. This value was approximately equal for H_2 and N_2. However, from the present results we conclude that other simplifying assumptions such as the introduction of a mean gas temperature and the mean temperature dependence of the diffusion coefficient evidently compensate for this effect.

Also, in the present model transport of material in the flow direction by axial diffusion of growth species was neglected. In principle, this should be taken into account by introducing a term $D(\partial^2 C(y, z)/\partial z^2)$ into the differential equation of mass conservation (eq. (1)). The solution of this problem, however, must be obtained numerically by computer calculations. Qualitatively, axial diffusion is expected to lower the concentration gradients in the z-direction, therewith decreasing the decay of growth rates downstream. In a first attempt to estimate the importance of this effect, mass transport by flow ($= v(y)C(y, z)$ and diffusion ($= -D(\partial C(y, z)/\partial z)$) were compared using the expression derived for the concentration profiles in the present model (eq. (8)) and the mean-temperature concept defined in eqs. (15)–(17). The results showed that under the presently used experimental conditions, in most cases the contribution of axial diffusion to the total transport of the active species in the flow direction was of the order 3–10%. This is considered to be negligible. Only for the case of H_2 in cell A where h is small, the effect was much stronger and amounted to tens of percents in the relevant range of z-values (fig. 7). Qualitatively, from a comparison of the slopes of the curves in figs. 5–7, it can also be concluded that the effect must be much larger in cell A with H_2 as a carrier gas than for the other experiments. As a typical example, the contribution of axial diffusion to the total mass transport in the z-direction in cell A with H_2 was calculated to be 40% and 15% at $y = h/16$ and $y = h/4$, respectively, for $z = z_0$ and an input flow velocity of 5 cm/s. Therefore, we conclude that the deviations between the experimental and calculated plots of the growth rate versus z in cell

A with H_2 as a carrier gas are mainly due to axial diffusion of reactants.

At higher gas velocities, some deviations from the model were observed for smaller values of z when N_2 was used as a carrier gas (fig. 6c). Additionally, in this region lateral variations in growth rates were observed to be much more pronounced than for larger values of z. From table 2 it is clear that these cases are characterized by relatively high Ra numbers approaching the critical value of 1700 in combination with long thermal entrance lengths covering a large part of the hot susceptor. Therefore, the above mentioned deviations can be attributed to instabilities in the entrance zone, which will be discussed in more detail in the next section.

The equations for the growth rate in a laminar flow system (eqs. (18) and (22)) are, in principle, only valid for the two-dimensional case of two semi-infinite parallel plates. A cell with a rectangular cross-section can also be considered as a two-dimensional system if the following requirements are fulfilled. First, lateral concentration gradients should be small, so as to minimize diffusion in this direction. Secondly, the gas flow velocity must be constant in the lateral direction. Finally, free convective motions which can cause differences in the supply of growth components laterally [15], should be unimportant. As to the first requirement, it was shown above that for a large part of the cell-width growth rates are constant (compare fig. 8). From this we infer that lateral diffusion effects will, at least in these regions, not play an important role. As to the second point, the gas velocity can be calculated as a function of lateral position x using an empirical expression derived by Holmes and Vermeulen [40]. The results are shown in fig. 14 for the four rectangular cells used in the present study. The tapered cell must be compared with cell B at the leading edge of the deposition zone and with cell A at the outlet position, $z = 20$ cm. The shapes of the profiles shown in fig. 14 strongly depend on the aspect ratio, b/h. For this discussion of results obtained in low Ra number systems, only cells A and B are relevant (table 2). For these cells, which have aspect ratios of 6.3 and 2.8, respectively, it can be seen in fig. 14 that the gas velocity is

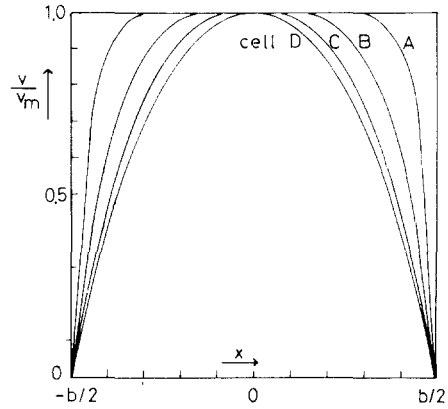

Fig. 14. Lateral distribution of gas velocities according to ref. [40] in the four rectangular cells used in the present study (A, B, C, D); v = gas velocity; v_m = maximum gas velocity for a specific height above the susceptor (y).

constant to within 5% in a region covering ~ 75% and ~ 50% of the total cell width, respectively. Growth rates were indeed observed to be constant within the experimental error in these regions. For cell B, the homogeneity was slightly better than theoretically expected for lower gas velocities (fig. 8a).

From these experimental results it is concluded that the lateral distribution of growth rates is determined by the lateral profile of the forced flow velocity in these low Ra number systems. This implies that free convective motions are not important. Giling's holographic experiments [6] showed that isotherms are perfectly parallel to the susceptor and gas flow patterns are very stable under the present conditions. From this it was concluded that in the part of the cell where flow and temperature profiles are developed, free convective motions are not important. Very recently, Houtman et al. [11] showed that still vortex rolls may be present in these systems. These motions, however, did not affect temperature distributions because of the high thermal conductivity of the hydrogen gas. Similarly, from the present work it can be concluded that if free-convective motions are present, they do not affect mass transport by diffusion and forced flow under low Ra number conditions. Therefore, for a consideration of growth rate distributions the flow may be assumed to be effectively forced laminar.

The results from this study show that depletion of the active growth component by homogeneous gas phase reactions is not important under the conditions which were presently used; such a mechanism would lead to other diffusion processes (e.g. Ga diffusion to the cold upper wall in case of top-cooling) and gas phase depletion characteristics. Partial decomposition of the TMG molecule in the gas phase can not be excluded, however, but the final step involving the formation of atomic Ga must occur at one of the hot walls (see also refs. [37,28,29]). Yoshida et al. [27] concluded that TMG decomposition in H_2 is a homogeneous first order reaction. Their results also can be explained, however, by a heterogeneous reaction and an equation similar to eq. (18). From the present results, no further conclusions can be drawn concerning the exact nature of the diffusing species. The differences which are expected in the diffusion coefficients of the various possible $Ga-Me_x$ species ($1 \leqslant x \leqslant 3$), do not allow further discrimination.

6.2. High Ra numbers: effective vortex formation

As was shown in section 5, for conditions characterized by high Ra numbers there is no good fit between the predictions from the present model and the experimental observations. The lateral variation of growth rates clearly shows the presence of strong vortex motions in the cell [15]. For cell D with H_2 as a carrier gas, in the entrance part of the deposition zone the lateral growth rate distribution is indicative of a negative vortex motion [15] (fig. 11) with a more effective supply of reactants at the centre of the cell. In the developed region, a positive vortex motion must be assumed with a lower growth rate in the centre of the cell. Such development of vortex motions is illustrated in the inserts in fig. 11: in the entrance region, negative vortex rolls predominate and positive rolls are generated near the side walls. The latter become more important for increasing z and are stable in the region where temperature and flow profiles are developed. These ideas are in accordance with results obtained from numerical computations by Houtman et al. [11].

The entrance length for a stable vortex motion to develop can be expected to be of the order of the entrance lengths for the velocity and temperature profiles. This was indeed experimentally observed (compare, e.g., table 2 and fig. 11). For the case of N_2 in cell B, as is demonstrated in fig. 12, a negative vortex motion is observed over the whole length of the cell. Possibly, this is caused by the long entrance lengths under these conditions (table 2), so that the positive vortices will only become predominant at z-values larger than the susceptor length. Alternatively, the temperature distribution at the cell boundaries may favour negative vortex motions. It should be noted that under comparable conditions Giling [6] also found a stable negative vortex for N_2 along the whole susceptor length, which is in agreement with the present observations.

In the entrance region, return flow of gas due to rapid expansion of cold gas hitting the hot susceptor [16,23] and so-called cold finger effects at high gas velocities [6] may also occur. Therefore, epitaxial layers should not be grown in this highly unstable region with possible large fluctuations in temperature, flow velocities and, consequently, growth rates. Another disadvantage of the return flow effects is the large gas memory which is introduced. This is a severe drawback when sharp heterojunctions have to be grown.

6.3. Characterization of the flow

From a comparison of the results obtained in systems with low and high Ra numbers, it can be concluded that this dimensionless number indeed provides a good criterion for the prediction of deposition characteristics. From the present results it can be concluded that the critical value must be between ~ 700 and ~ 1700 to 2800. This is in reasonable agreement with the critical value of ~ 1700, which was defined in previously published theoretical and experimental work [6,34,35]. Some authors [3,5] suggested to use the ratio of Grashof number and squared Reynolds number, Gr/Re^2, to describe the flow characteristics. In the present work no relation between the flow and deposition characteristics and this ratio was found. Table 2 shows, for example, that the value of Gr/Re^2 is equal for H_2 and N_2 in cell B. How-

ever, the growth rate distributions in this cell and, consequently, flow characteristics are markedly different (figs. 5, 8 and 12). These were concluded to be dominantly forced laminar and free convective with vortex formation, respectively. In addition, for cell A the Gr/Re^2 ratio predicts a mixed flow for all conditions presently used (ref. [3], table 2). Lateral growth rate distributions, however, could be explained by assuming forced laminar flow characteristics under all conditions. Therefore, we conclude that the Gr/Re^2 ratio does not provide a good criterion to describe the flow and deposition characteristics.

6.4. Remarks on cell design

In the present work, only cells with rectangular cross-sections were used. The main reason for this was that in such cells temperature gradients across the susceptor width are minimized [6]. Thus, by using a top-cooling, a very stable pattern of isotherms running parallel to the susceptor can be obtained under forced laminar conditions. From the growth results it can be stated that flow conditions characterized by high Ra numbers ($> \sim 1700$) should be avoided, because apart from instabilities and return flow effects in the entrance region, lateral growth rate variations are large for all axial positions due to strong (free-convective) vortex motions.

To minimize unwanted gas phase depletion, the cell should be top-cooled at a temperature below $\sim 350°C$. Above this value, TMG decomposition is initiated [27]. In the present work, water top-cooling (~ 300 K) was used. When growing thick GaAs layers, however, in some cases dust problems appeared for larger values of z due to an accumulation of arsenic condensates at the cold upper wall. Most probably, this can be avoided to a large extent by using a higher top-cooling temperature. This may have additional advantages, such as a lowering of the Ra number and a decrease of arsenic memory effects when growing multilayer structures with varying V elements. These effects will be subject to future studies.

In order to obtain a constant layer thickness on large surface areas, two further requirements should be fulfilled. A constant growth rate in the axial direction can be obtained when a tapered cell, or, alternatively, a titled susceptor, is used in combination with the proper gas velocity (eq. (23). Good lateral homogeneity over 70% of the cell width can be achieved when the aspect ratio b/h is larger than ~ 4.

A special problem may arise when ternary or quaternary III–V crystals containing more than one III element are grown by MOCVD. If these III elements diffuse independently to the hot susceptor, also the gas phase depletion of these species will be independent. As a consequence, compositional grading of the epitaxial layers may be expected in the axial direction (z) in such cases if the diffusion coefficients of the species involved are quite different. The same remark can be made for dopants, when their incorporation in the epitaxial layers is diffusion controlled. These effects will also be subject to a future study.

It should be noted that apart from the specific recommendations discussed here, general considerations of flow dynamics should be taken into account when constructing a reactor cell, including minimization of dead spaces, avoiding obstacles which can produce flow eddies and, for the same reason, minimization of angles when dimensions are changed ($< \sim 10°$; see, e.g., refs. [23,41]). Those factors become especially important when multilayer structures with sharp interfaces have to be grown, because they may cause severe memory effects.

7. Conclusions

From this work the following conclusions for horizontal epitaxial cells can be drawn.

(1) For the characterization of flow:

- The Rayleigh number is a good criterion for the characterization of the flow and growth rate distributions under non-turbulent ($Re < 2300$) conditions, both for H_2 and N_2; for $Ra < \sim 700$ (this work) the flow is dominantly forced laminar; for $Ra > \sim 1700$–2800 (this work) free convective effects are important and strong vortex motions are present. Large entrance effects are often observed;
- The Gr/Re^2 ratio is not a reliable measure to characterize the flow.

(2) As regards the present theoretical model:

– A good fit between experimental MOCVD results and calculations on the basis of the model was obtained for low Ra number systems ($< \sim 700$), both with N_2 and H_2 as carrier gases; this gives further proof that the growth in MOCVD is indeed controlled by diffusion of the III component.
– For high Ra numbers no good fit could be obtained. Due to vortex motions supply of reactants can be increased or decreased, locally. Growth rates at the centre of the susceptor were found to decay exponentially after the thermal entrance region, but effective boundary layers with which such behaviour can be described have no physical reality.
– In diffusion-controlled systems a concentration entrance length can be important, especially for higher flow velocities. Here, growth rates do not decay exponentially with the axial position, but (as follows from the present model) with a $1/3$ power law.

(3) TMG decomposition mechanism in MOCVD:
– TMG decomposition is not complete in the gas phase. At least, removal of the last methyl group must occur at a hot, $\geqslant \sim 700$ K, cell boundary. This conclusion supports other previous MOCVD work [37,28,29].

(4) Cell design for growth of layers with a constant thickness on large surfaces:
– Low Ra number conditions should be chosen.
– A top-cooled cell should be used to minimize depletion on the relatively hot, air-cooled, top.
– A tapered cell (or tilted susceptor), in combination with the proper gas velocity, will give excellent axial growth rate homogeneity.
– Aspect ratios larger than ~ 4 will provide good lateral growth rate homogeneity for over 70% of the susceptor width.

A general conclusion from this work is that a study of growth rate distribution as a function of place on the susceptor can give very valuable information on properties of the flow and the epitaxial growth mechanism.

Acknowledgements

The authors would like to thank Mr. J.J.C. Holten and Mr. P.P. Coelen for construction of some of the cells under high time pressure. This work was performed as a part of the research programme of the "Stichting voor Fundamenteel Onderzoek der Materie" (FOM) with financial support from the "Nederlandse Organisatie voor Zuiver Wetenschappelijk Onderzoek" (ZWO).

References

[1] G.J. Hwang and K.C. Cheng, J. Heat Transfer ASME 95 (1973) 72.
[2] Y. Kamotami and S. Ostrach, J. Heat Transfer ASME 98 (1976) 62.
[3] E.M. Sparrow, R. Eichhorn and J.L. Gregg, Phys. Fluids 2 (1959) 319.
[4] V.S. Ban and S.L. Gilbert, J. Crystal Growth 31 (1975) 284.
[5] V.S. Ban, J. Electrochem. Soc. 125 (1978) 317.
[6] L.J. Giling, J. Electrochem. Soc. 129 (1982) 634.
[7] L.J. Giling, J. Physique 43 (1982) C5-235.
[8] M. Koppitz, O. Vestavik, W. Pletschen, A. Mircea, M. Heyen and W. Richter, J. Crystal Growth 68 (1984) 136.
[9] J. Juza and J. Cermák, J. Electrochem. Soc. 129 (1982) 1627.
[10] M.E. Coltrin, R.J. Kee and J.A. Miller, J. Electrochem. Soc. 131 (1984) 425.
[11] C. Houtman, H. Moffat and K.F. Jensen, in: Proc. 6th European Conf. on CVD, Uppsala, 1985, p. 73.
[12] J. Bloem and L.J. Giling, in: Current Topics in Materials Science, Vol. 1, Ed. E. Kaldis (North-Holland, Amsterdam, 1978) ch. 4, p. 147.
[13] F.C. Eversteyn, P.J.W. Severin, C.H.J. van den Brekel and H.L Peek, J. Electrochem. Soc. 117 (1970) 925.
[14] G.B. Stringfellow, J. Crystal Growth 68 (1984) 111.
[15] R. Takahashi, Y. Koga and K. Sugarawa, J. Electrochem. Soc. 119 (1972) 1406.
[16] L.J. Giling, J. van de Ven and H.H.C. de Moor, unpublished "in situ" results, 1985.
[17] B.I. Boltaks, in: Diffusion in Semiconductors, Ed. H.J. Goldsmit (Infosearch, London, 1963) pp. 107–109.
[18] R.B. Bird, W.E. Stewart and E.N. Lightfoot, Transport Phenomena (Wiley, New York, 1966) p. 551.
[19] E.R.G. Eckert, J. Aeronautical Sci. 22 (1955) 585.
[20] J. Hitchman, J. Crystal Growth 48 (1980) 394.
[21] K. Chen, J. Crystal Growth 70 (1984) 64.
[22] S. Berkman, V.S. Ban and N. Goldsmith, in: Heteroepitaxial Semiconductors for Electronic Devices, Eds. G.W. Cullen and C.C. Wang (Springer, New York, 1978) p. 264.
[23] L.J. Giling, presented at 6th Intern. Conf. on Vapor Growth and Epitaxy, Atlantic City, NJ, July 1984.
[24] H. Schlichting, Boundary-Layer Theory, 6th ed. (McGraw-Hill, New York, 1968) pp. 177–178.
[25] J.L. Weyher, in: Proc. 4th European Conf. on CVD, Eindhoven, 1983, p. 273.
[26] M. Razeghi, B. de Crémoux and J.P. Duchemin, J. Crystal Growth 68 (1984) 389.

[27] M. Yoshida, H. Watanabe and F. Uesugi, J. Electrochem. Soc. 132 (1985) 677.
[28] J. van de Ven, H.G. Schoot and L.J. Giling, J. Appl. Phys., in press.
[29] M. Mizuta, T. Iwamoto, F. Moriyama, S. Kawata and H. Kukimoto, J. Crystal Growth 68 (1984) 142.
[30] R.H. Persy, C.H. Chilten and S.D. Kirchpatrick, Perry's Chemical Engineering Handbook, 4th ed. (McGraw-Hill, New York, 1969) pp. 19–21.
[31] Texas Alkyls, "Product Data" TMG (1983).
[32] W.M. Kays and M.E. Crawford, Convective Heat and Mass Transfer, 2nd ed. (McGraw-Hill, New York, 1980) pp. 389–390.
[33] H. Schlichting, Boundary Layer Theory, 6th ed. (McGraw-Hill, New York, 1968) p. 432.
[34] H.H. Sogin and H.A. Thompson, in: Proc. 5th Symp. on Thermophysical Properties, Newton, MA, Oct. 1970.
[35] B.J. Curtis and J.P. Dismukes, J. Crystal Growth 17 (1972) 128.
[36] J. van de Ven, J.L. Weyher and G.M.J. Rutten, presented at 2nd Intern. Conf. on Metalorganic Chemical Vapour Deposition, Sheffield, April 1984.
[37] D.H. Reep and S.K. Ghandhi, J. Electrochem. Soc. 130 (1983) 675.
[38] J. Bloem, J. Electrochem. Soc. 117 (1970) 1397.
[39] K.E. Grew and T.L. Ibbs, Thermodiffusion in Gases (Cambridge University Press, Cambridge, 1952).
[40] D.B. Holmes and J.R. Vermeulen, Chem. Eng. Sci. 23 (1968) 717.
[41] H. Schlichting, Boundary Layer Theory, 6th ed. (McGraw-Hill, New York, 1968) pp. 28–36.